Organic Electronics 9 (2008) 1010–1016

Contents lists available at ScienceDirect

Organic Electronics

journal homepage: www.elsevier.com/locate/orgel

# Influence of 2-mercapto-5-nitrobenzimidazole treatment on the electronic characteristics of bottom-contact organic field-effect transistors

D.S. Park [a], W.C. Jang [a], S.W. Cho [a], J.H. Seo [a,1], I.S. Jeong [a], T.W. Kim [b], G.S. Chang [c,*], A. Moewes [c], K.H. Chae [d], K. Jeong [a], K.-H. Yoo [a], C.N. Whang [a,*]

[a] Institute of Physics and Applied Physics, Yonsei University, Seoul, 120-749, Republic of Korea
[b] Department of Physics, Hongik University, Seoul 121-791, Republic of Korea
[c] Department of Physics and Engineering Physics, University of Saskatchewan, Saskatoon, SK, Canada S7N 5E2
[d] Division of Materials Science and Technology, Korea Institute of Science and Technology, Seoul 130-791, Republic of Korea

ARTICLE INFO

*Article history:*
Received 11 April 2008
Received in revised form 4 July 2008
Accepted 20 July 2008
Available online 7 August 2008

*PACS:*
61.66.Hq
72.80.Le
73.61.Ph
78.70.Dm
78.70.En

*Keywords:*
Pentacene
Field-effect transistors
2-mercapto-5-nitrobenzimidazole
Self-assembled monolayer

ABSTRACT

The treatment of the Au electrodes of an organic bottom-contact thin film transistor with 2-mercapto-5-nitrobenzimidazole (MNB) led to improved current–voltage characteristics. X-ray diffraction, atomic force microscopy, soft X-ray emission spectroscopy, and ultraviolet photoelectron spectroscopy were used to investigate the structure-function relationship in the device components MNB and pentacene. By treating the Au contacts with MNB prior to the pentacene deposition, the morphological and structural properties of the pentacene come to resemble the ideal case of pentacene deposited onto $SiO_2$. The action of the MNB is therefore to remove the transition region at the Au/pentacene interface, leading to improved charge carrier injection.



## 1. Introduction

Thin-film transistors (TFTs) based on organic semiconductors have wide applicability in optoelectronics and sensor technologies, including active-matrix organic displays [1–3], electronic-paper technology [4], and radio-frequency identification circuitry [5], and there is growing interest in the development of highly integrated circuits based on this technology. Pentacene is regarded as a suitable material for this application because its field-effect mobility and drain-current on-off ratio are comparable to that of amorphous Si [6–9]. Pentacene-based TFT devices can be fabricated in either top- or bottom-contact structure; the latter one is easier to produce through photolithography processes due to the intolerance of organic materials to the chemical etchants that are typically used in the lithographic patterning processes. The downside to the bottom-contact thin film transistor (BC-TFT) architecture is that their electronic characteristics are inferior to those of top-contact TFTs (TC-TFTs) [10–12].

The fabrication of pentacene BC-TFT devices requires that an active pentacene layer deposited onto both the $SiO_2$ gate insulator and the Au electrodes. The high surface

* Corresponding author. Tel.: +1 306 966 2768; fax: +1 306 966 6400.
*E-mail addresses:* gapsoo.chang@usask.ca (G.S. Chang), cnwhang@yonsei.ac.kr (C.N. Whang).
[1] Present address: Center for Organic and Polymers Solids, Department of Chemistry and Biochemistry, University of California, Santa Barbara, CA 93106, USA.

1566-1199/$ - see front matter © 2008 Elsevier B.V. All rights reserved.
doi:10.1016/j.orgel.2008.07.012

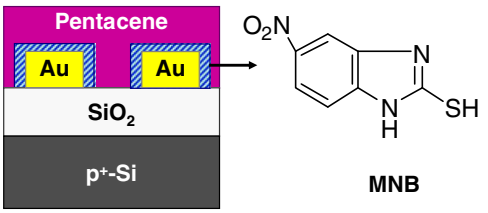


**Fig. 1.** The cross-sectional schematic of a pentacene BC-TFT with MNB-treated Au electrodes. The molecular structure of MNB is given in the right.

energy of the Au surface leads to poor morphology and crystalline quality of the pentacene layer, leading to the formation of a transition layer that degrades the device characteristics of pentacene BC-TFT devices [5,10]. This difficulty can be overcome through passivation of the Au layer, allowing the pentacene layer to be uniform throughout the device. Deposition of a self-assembled monolayer (SAM) onto the Au electrodes has been shown to modify the interface between the electrode and the active organic materials [3,8,13–15] and is a useful technique for improving the device characteristics. Especially, it has been reported that treating the Au electrode using 2-mercapto-5-nitro-benzimidazole (MNB) reduces contact resistance by 20–50% and significantly improve the field-effect mobility [16,17].

In this paper, we present a study of the effects of depositing a MNB–SAM onto the Au electrodes of a pentacene BC-TFTs. The structure of MNB allows the Au surface to be thiolated while leaving the active site at the opposite end of the MNB available for bonding to the pentacene (see Fig. 1). Our results show that when a pentacene thin film is deposited onto MNB-treated Au electrodes, the current–voltage (*I–V*) characteristics are significantly enhanced. We determine the structural basis for this modification of the device characteristics by examining the morphology and crystalline structure of pentacene in untreated and MNB-treated BC-TFTs using atomic force microscopy (AFM) and X-ray diffraction (XRD). In addition, the modifications of the unoccupied and occupied molecular orbitals that are associated with charge-transport in pentacene were examined using soft X-ray spectroscopy.

## 2. Experimental

A 100 nm-thick $SiO_2$ layer was synthesized on a heavily doped $p^+$-Si substrate using a dry oxidation process. Subsequently, the source and drain electrodes were deposited by thermally evaporating a 15 nm layer of Au at a pressure of $5 \times 10^{-8}$ Torr using a shadow mask. The channel length ($L$) and width ($W$) for the electrodes were 50 μm and 1000 μm respectively. A 10 nm-thick MNB layer was evaporated onto the Au electrodes at a deposition rate of 0.01 nm/s. The MNB-deposited sample was washed in acetone in order to remove the excess MNB from the Au and $SiO_2$ surface. Through this process, only the MNB molecules that are bonded to the Au surface are left; the MNB is completely removed from the TFT channel and does not affect the pentacene/$SiO_2$ interface. The $SiO_2$ surface was inspected with an AFM to confirm that the MNB had been removed. The thermal evaporation of a 100 nm-thick pentacene active layer was then conducted at 165 °C at a base pressure of $5 \times 10^{-9}$ Torr. The deposition rate and substrate temperature were maintained at 0.05 nm/s and room temperature, respectively. Fig. 1 shows the cross-sectional schematic of our pentacene BC-TFTs with MNB-treated Au electrodes. For comparison purposes pentacene BC-TFTs without any treatment were also prepared in the same manner.

The *I–V* characteristics of the BC-TFTs were measured using two Keithley 2400 source measurement units. The crystalline structure of the pentacene was confirmed by recording the $\theta$–$2\theta$ XRD patterns with an incident X-ray wavelength of 1.5425 Å at beamline 10C1 of the Pohang Light Source at the Pohang Accelerator Laboratory. The C 1*s* X-ray absorption (XAS) and C $K\alpha$ X-ray emission (XES) spectra were obtained at beamline 8.0.1 of the Advanced Light Source at the Lawrence Berkeley National Laboratory. The spectra were normalized to the number of photons falling on the sample which was monitored by measuring the photocurrent produced in a highly transparent Au mesh located just upstream of the sample chamber. The charge transfer in our devices was studied by comparing MNB-treated and untreated Au layers that had been prepared for *in situ* ultraviolet photoelectron spectroscopy (UPS) measurements. Several thicknesses of pentacene (0.1, 0.2, 0.4, 0.8, 1.6, 3.2, 6.4, and 25.6 nm) were measured in regular order without breaking vacuum by depositing them in a sample preparation chamber attached to the analysis chamber. The UPS spectra were measured using He I sources with a hemispherical electron energy analyzer (PHI 5700 spectrometer) with −15 V of sample bias, and the analysis chamber and sample preparation chamber were maintained at $1 \times 10^{-10}$ and $1 \times 10^{-9}$ Torr, respectively.

## 3. Results and discussion

The *I-V* characteristics in Fig. 2 demonstrate the superior electronic characteristics of the BC-TFT device fabricated with MNB-treated Au electrodes, as compared to the untreated pentacene BC-TFT; the characteristics are summarized in Table 1. The maximum drain current ($I_D$) of the MNB-treated transistor, recorded with both drain ($V_D$) and gate ($V_G$) voltages at −40 V, is −16 μA – two orders of magnitude larger than that of the untreated transistor (see Fig. 2b). The influence of MNB-treatment on the carrier-transport characteristics can be determined from the $(-I_D)^{1/2}$ versus $V_G$ plots ($V_D = -40$ V) in Fig. 2c and d. All plots are taken at $V_D = -40$ V. The $(-I_D)^{1/2}$ versus $V_G$ relation is generally governed by [7]:

$$I_D = \frac{WC_i}{2L}\mu(V_G - V_{TH})^2, \quad (1)$$

where $\mu$ is the field-effect mobility, $V_{TH}$ is the threshold voltage, and $C_i$ is the capacitance of the $SiO_2$ gate insulator. The value of $\mu$ can be extracted from Eq. (1), and so we estimate the field-effect mobility of the MNB-treated pentacene BC-TFT to be 0.14 $cm^2$/Vs, an order of magnitude larger than the value determined for the untreated transistor (0.0064 $cm^2$/Vs). The subthreshold swings (*SS*) can also determined from the logarithmic $-I_D$ versus $V_G$ plots by comparison with the model equation [7]:

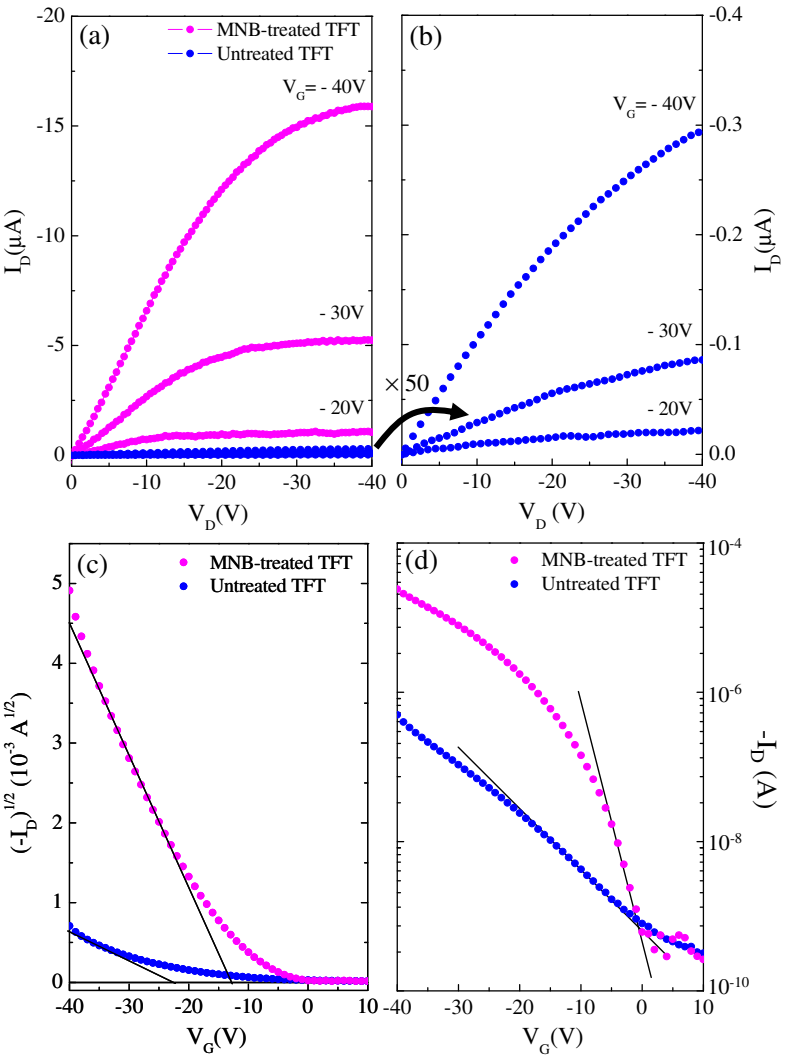


**Fig. 2.** (a) Plots of drain current ($I_D$) versus drain voltage ($V_D$) of untreated (pink circle) and MNB-treated pentacene BC-TFTs (blue circle) for various gate voltages ($V_G$) and (b) corresponding plots of untreated BC-TFTs at 50 times magnification. (c) Plots of the square root of $-I_D$ versus $V_G$ and (d) logarithmic plots of $-I_D$ versus $V_G$ of untreated and MNB-treated pentacene BC-TFTs.

**Table 1**
Summary of the device characteristics of untreated and MNB-treated pentacene BC-TFTs

| Sample | $\mu$ ($cm^2$/Vs) | Maximum $I_D$ (A) | On/off ratio | *SS* (V/decade) | $V_{TH}$ (V) |
|---|---|---|---|---|---|
| Untreated BC-TFT | 0.0064 | $-2.9 \times 10^{-7}$ | $2 \times 10^3$ | −12.88 | −21.5 |
| MNB-treated BC-TFT | 0.14 | $-1.6 \times 10^{-5}$ | $7 \times 10^4$ | −3.17 | −12.6 |

$$SS = \frac{dV_G}{d\log(-I_D)}. \quad (2)$$

Analyzing the curves in Fig. 2d, we can see that treatment of the electrodes with MNB reduces the *SS* from −12.88 V/decade in the untreated BC-TFT to −3.17 V/decade. The influence of the MNB–SAM treatment on the BC-TFT device characteristics is clear, and the following analysis will illuminate the structural and electronic effects that lead to these enhancements.

The carrier-transport characteristics of the organic active layer of these devices are related to the morphology and structure of the pentacene, specifically the crystallinity of the pentacene and the degree to which the layers on the Au electrodes match that on the $SiO_2$ gate dielectric [9,15–18]. Fig. 3 shows the AFM images of pentacene layers deposited on: (a) MNB-treated Au, (b) untreated Au, (c) $SiO_2$ on which MNB was deposited and subsequently dissolved from, and (d) clean $SiO_2$. The insets show the roughness profiles of each pentacene film. Importantly, there is no noticeable morphological difference between the pentacene films on the clean $SiO_2$ surface and the surface from which the MNB has been dissolved, confirming that the influence of the MNB treatment of the BC-TFT devices is confined to the Au electrodes. This is in accordance with

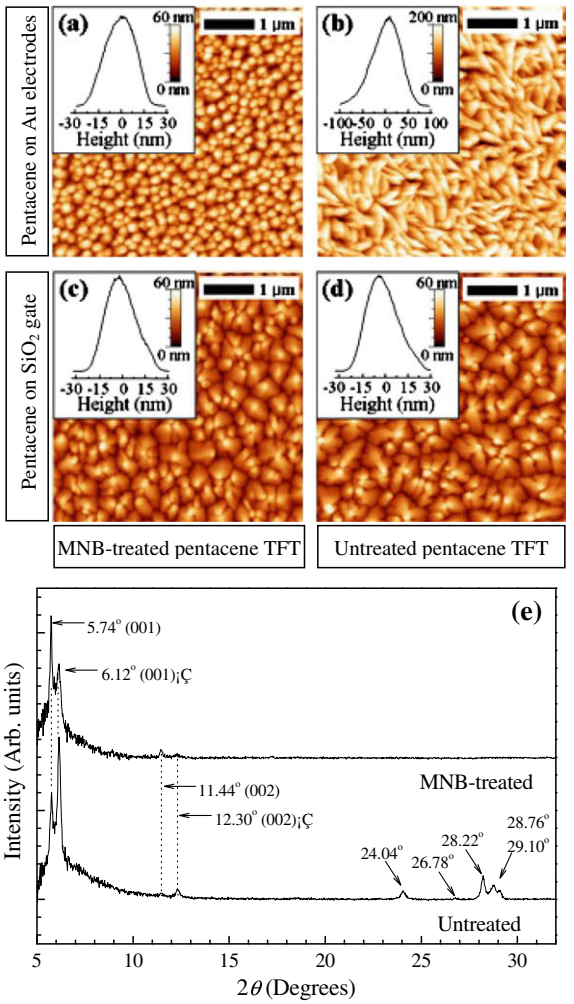


**Fig. 3.** AFM images of pentacene thin films on various substrates: (a) on MNB-treated Au, (b) on untreated Au, (c) on MNB dissolved $SiO_2$ after MNB deposition, and (d) on clean $SiO_2$. The insets represent the roughness profile of the pentacene surface. (e) XRD patterns of pentacene thin films on MNB-treated and untreated Au surfaces.

other reports suggesting that thiol compounds are selectively self-assembled onto the Au electrodes due to nondissociative adsorption of thiol (S-H) groups [19,20]. Depositing the MNB–SAM on the Au surface prior to the pentacene deposition causes the resultant film of round-shaped grains to have roughness similar to that of the film on the $SiO_2$ surfaces. The size and shape of the grains are quite similar to the films grown on OTS-treated $SiO_2$ substrates with highly-packed grain boundaries in a previous report [21]. The absence of the MNB–SAM has a pronounced effect on the morphology of the pentacene film deposited on the Au substrate, which has a rough surface characterized by rod-shaped grains. The effect of the MNB–SAM treatment on the morphology of the pentacene layer correlates with the variations in electronic characteristics described above, adding more evidence that the charge injection into the pentacene layer is improved as a result of structural modifications induced by the treatment of the Au electrodes.

The crystal phases of the pentacene films deposited on Au surfaces, both treated and untreated, is reflected in the XRD patterns shown in Fig. 3e. Both pentacene films are a mixture of the thin-film and the single-crystal phases described by Dimitrakopoulos et al. [9]. The structure of pentacene single crystals adopt the triclinic ($P1$ group) with the (0 0 1) plane spacing ($d_{001}$) of 14.5 Å, while the $d_{001}$ of pentacene thin-films equals 15.4 Å. Although it has recently been shown that the thin-film phase is not entirely independent of the substrate identity [18], the values obtained here are very close to what has been reported for pentacene on other surfaces. The diffraction peak at 5.74° (and 11.44° for the second-order diffraction) corresponds to a $d_{001}$ spacing equal to 15.4 Å, showing evidence for the thin-film phase, while the peak at 6.12° (12.3°) corresponds to $d_{001}$ = 14.5 Å from the single-crystal phase. It is clear that the thin-film phase is dominant in the pentacene film grown on MNB-treated Au, as in the pentacene thin film on $SiO_2$ surface. In addition to the alignment of the pentacene molecules along the long axes of 14.5 Å and 15.4 Å, the pentacene films grown on the bare Au surface exhibit several more diffraction peaks at 24.04°, 26.78°, 28.22°, 28.76°, and 29.10°, corresponding to a much lower plane-spacing of about 3 Å. The peaks with high Bragg angles come from the first monolayer of pentacene molecules on bare Au surface lying almost parallel to the Au surface; these peaks do not appear in the XRD patterns measured from the pentacene on the MNB-treated Au surface or on the $SiO_2$ surface [10,11]. The dominant presence of the thin film phase and the absence of the flat-lying phase are characteristic of the pentacene film deposited on the treated Au surface, demonstrating the relationship between the quality of the crystalline structure and the improved device characteristics that are brought about by the MNB–SAM electrode treatment.

Taking the above morphological and structural results into account, it is quite clear that changes in electrode surface energy occur in the pentacene BC-TFTs owing to the MNB treatment, and that this change enhances the packing of pentacene grains, making them similar to what is observed on $SiO_2$. A more highly-packed pentacene grains at the Au electrodes' surfaces leads to the reduction of grain boundary scattering, resulting in better charge-transport characteristics and a smooth pentacene surface contribute to the enhancement of injection efficiency. Since the injection and transport of charge carriers in TFT devices are strongly related to the delocalized molecular orbital states of the organic layer, we expect to see evidence of a correlation between the device properties and the molecular orbital states of pentacene films deposited on treated and untreated Au surfaces.

The partial density of the unoccupied carbon 2$p$ molecular orbital states of pentacene is probed by the C 1$s$ XAS spectra shown in Fig. 4a. The $\pi^*$ states are represented by the sharp resonant absorption features in the region 283–287 eV; the broad features in the region above 288 eV are $\sigma^*$ resonances. The location of the lowest unoccupied molecular orbital (LUMO) is marked by a vertical line at 284.1 eV. As is expected from the previous structural and functional characterization, the C 1$s$ XAS spectrum of the pentacene thin film on MNB-treated Au

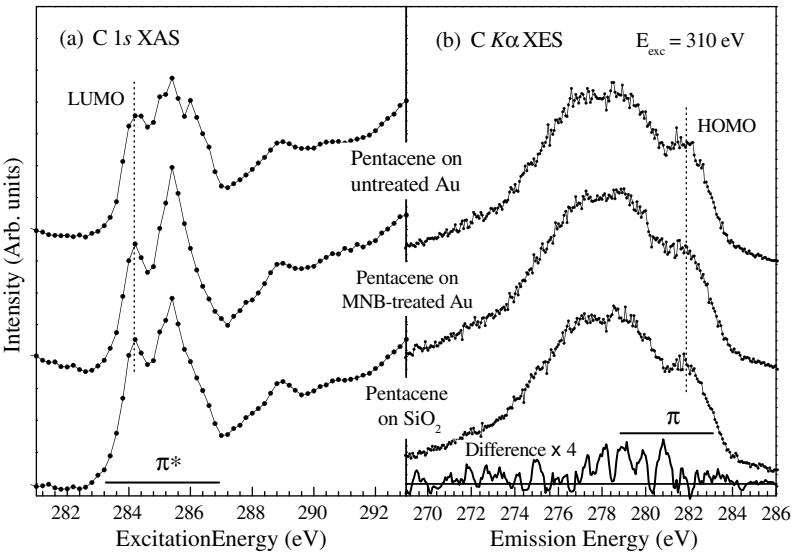


**Fig. 4.** (a) C 1*s* XAS spectra of pentacene thin films on MNB-treated Au, untreated Au, and $SiO_2$ substrates and (b) C *K*α non-resonant XES spectra of corresponding samples excited at 310 eV.

resembles that of well-ordered pentacene films on $SiO_2$ substrates. Since the incident angle of linearly polarized X-rays was set to 30° with respect to the sample's normal direction, the XAS measurements mostly probe the *p*-characteristics of the molecule parallel to the sample surface. Therefore, two intense features at 284.2 and 285.4 eV suggest that unoccupied $\pi^*$ orbitals are aligned nearly parallel to the plane of the sample's surface. This agrees well with results for pentacene films grown on SAM-modified Au surfaces reported by Hu et al. [11]. For pentacene films grown on untreated Au, the spectrum exhibits some additional features at 285 and 286 eV. These sub-features most likely stem from a different packing arrangement of the pentacene molecules. As seen in Fig. 3, a pentacene film deposited on Au contains randomly-oriented grains possessing rod-like shapes. By examining the spectral features is therefore able to determine the various pentacene alignments present in the samples.

The C *K*α XES spectra in Fig. 4b describe the partial density of the occupied molecular orbitals. The excitation energy ($E_{exc}$) was set to 310 eV, well above the absorption threshold, in order to ensure that the X-ray absorption and emission processes are entirely decoupled and the resulting fluorescence spectra is free from resonant scattering effects. The emission from transitions originating from the highest occupied molecular orbital (HOMO) occurs at 281.8 eV, marked with a vertical line. One can see that there is a discernable increase in π orbital states around 279–281 eV when pentacene is deposited on MNB-treated Au. This π-state enhancement is highlighted in the bottom spectrum which is obtained by subtracting the spectrum of pentacene film on untreated Au from that on the MNB-treated Au. Before the subtraction, all spectra were normalized to the number of photons falling on the sample monitored by the photocurrent of a highly transparent gold mesh. The delocalization boundary of π molecular states is enlarged as their binding energy increases [12]. Therefore the enhancement of π orbital states at lower emission energy (higher binding energy) represents a large intermolecular overlapping of π orbitals. These spectroscopic results provide excellent evidence in explaining the superior electronic characteristics found for MNB-treated pentacene BC-TFTs in comparison to those of untreated BC-TFTs.

For further evaluation of the electronic structure at the interface of the pentacene and the treated or untreated Au surfaces, UPS measurements were performed. Although it is a surface-sensitive technique, the UPS spectra of various thicknesses of pentacene (Fig. 5) demonstrate a clear effect of the MNB–SAM treatment on the electronic structure of the organic active layer. A double-stepped high binding energy cutoff ($E_{cutoff}$) is observed in the UPS spectra of pentacene on MNB-treated Au. This phenomenon is a spectral signature caused by MNB molecules bonded to Au molecules and also to exposed, unbounded Au, both of which are detectable because complete surface coverage cannot be obtained. There is a clear shift in $E_{cutoff}$ as a function of pentacene thickness on both MNB-treated and untreated Au. The direction of shifts are opposite, however; on MNB-treated Au the pentacene $E_{cutoff}$ shifts towards lower binding energy with increasing thickness, while the opposite shift occurs for pentacene on untreated Au. The $E_{cutoff}$ shifts at maximum pentacene coverage (25.6 nm) are −0.59 eV and 1.07 eV on MNB-treated and untreated Au, respectively. These results indicate that the vacuum level of pure pentacene is higher than that of MNB-treated Au but lower than that of untreated Au, and so a dipole is formed at each interface. The dipole has an opposite direction in the two cases, however, which has a direct effect on the device characteristics. The reversal of the interfacial dipole as a result of the MNB–SAM treatment of the Au comes about as a result of the change in Au surface energy, and provides a direct indication of the treatment's effect on the electronic characteristics of the device [22].

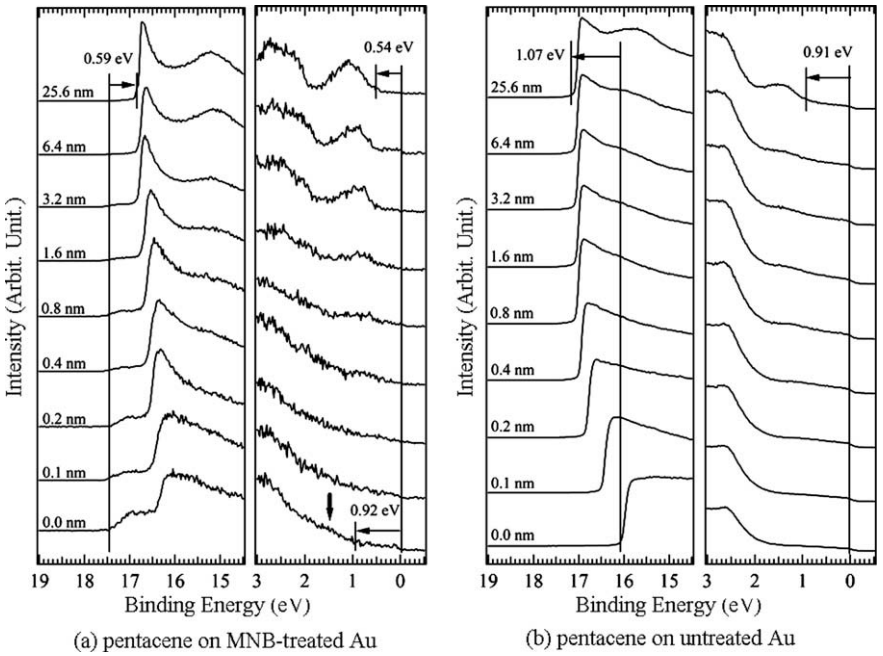


**Fig. 5.** UPS spectra of a series of thicknesses of pentacene (0.1, 0.2, 0.4, 0.8, 1.6, 3.2, 6.4, and 25.6 nm) (a) on MNB-treated Au and (b) on untreated Au.

The HOMO region (0–3 eV) is displayed in Fig. 5 on a binding energy scale relative Fermi energy level ($E_F$). Once the pentacene thickness has reached 3.2 eV there is a clear signal from the HOMO level. The gaps between $E_F$ and the HOMO onset of pentacene can thus be determined to be 0.54 eV and 0.91 eV on MNB-treated Au and on untreated Au, respectively. The reduction in the gap as a result of the MNB–SAM deposition reflects the lowering of the height of the injection hole injection barrier, coinciding with the reduced *SS* of the BC-TFT that was fabricated with MNB-treated Au electrodes. In addition, the HOMO level of MNB can be observed in the spectra of MNB-treated Au without pentacene deposition (0.0 nm pentacene thickness); it is found at 0.92 eV relative to $E_F$ and is indicated with an arrow at Fig. 5a. The agreement between the MNB and pentacene HOMO levels ensures that there is

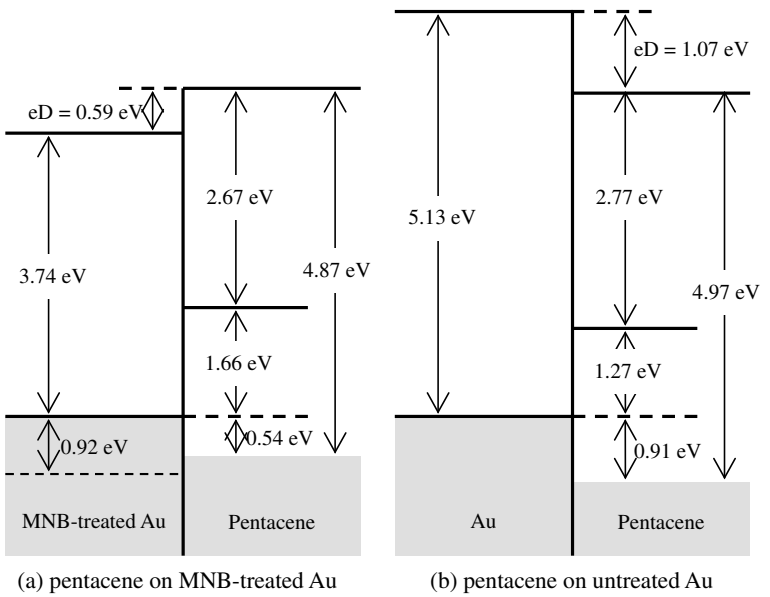


**Fig. 6.** Band diagrams of pentacene (a) on MNB-treated Au and (b) on untreated Au.

an efficient coupling between the two, and that no hole injection barrier exists at the pentacene/MNB interface [23].

The information provided by the UPS spectra can be summarized and interpreted in terms of the energy diagram for pentacene/MNB/Au that is shown in Fig. 6. The energy of the LUMO of pentacene was determined in relation to the HOMO level by adding the value of a previously-reported HOMO–LUMO gap (2.2 eV) [24]. The ionization potential ($I_P$) of pentacene is determined from the UPS spectra by using the following equation:

$$I_P = h\nu - E_{cutoff} + E_{HOMO}, \quad (3)$$

where $h\nu$ indicates the incident photon energy of 21.2 eV, and $E_{HOMO}$ is the onset energy of the HOMO level. According to the equation, the $I_P$ of pentacene on MNB-treated Au and on untreated Au are 4.87 eV and 4.97 eV, respectively. The slight decrease in the $I_P$ of pentacene on MNB-treated Au is attributed to the increasing delocalization of $\pi$ molecular states.

## 4. Conclusions

We have investigated the influence of a MNB treatment on the electronic characteristics of pentacene thin film transistors fabricated with a bottom-contact structure. The *I-V* characteristics of the BC-TFT devices are greatly improved by the treatment of the Au electrodes with an MNB–SAM prior to the deposition of the pentacene active layer. The morphological and spectroscopic investigations reveal a strong correlation between the enhanced electronic characteristics and the structural and morphological changes brought about by the MNB–SAM treatment. The treatment causes the pentacene layer on the Au electrode to closely resemble that of the layer deposited on the $SiO_2$ gate dielectric, eliminating any transition regions and accompanying barriers. The close-packed grains and enhanced molecular order of the pentacene film gives rise to the improvement of carrier-transport characteristics, leading to more efficient device performance. The presence of the MNB layer also reduces the injection barrier at the interface between the electrode and the pentacene, which improves the device performance as well.

## Acknowledgements

This work was supported by the Brain Korea 21 (BK21) project of the Korea Research Foundation (KRF), and the Korea Science and Engineering Foundation (KOSEF) through the National Core Research Center for Nanomedical Technology. We gratefully acknowledge the Natural Sciences and Engineering Research Council of Canada and the Canada Research Chair program.

## References

[1] H.E.A. Huitema, G.H. Gelinck, J.B.P.H. van der Putten, K.E. Kuijk, K.M. Hart, E. Cantatore, D.M. de Leeuw, Adv. Mater. 14 (2002) 1201.
[2] C.D. Sheraw, L. Zhou, J.R. Huang, D.J. Gundlach, T.N. Jackson, M.G. Kane, I.G. Hill, M.S. Hammond, J. Campi, B.K. Greening, J. Francl, J. West, Appl. Phys. Lett. 80 (2002) 1088.
[3] K. Nomoto, N. Hirai, N. Yoneya, N. Kawashima, M. Noda, M. Wada, J. Kasahara, IEEE Trans. Elect. Dev. 52 (2005) 1519.
[4] R. Wisnieff, Nature 394 (1998) 225.
[5] P.F. Baude, D.A. Ender, M.A. Haase, T.W. Kelley, D.V. Muyres, S.D. Theiss, Appl. Phys. Lett. 82 (2003) 3964.
[6] J.M. Shaw, P.F. Seidler, IBM J. Res & Dev. 45 (2001) 3.
[7] D.A. Neamen, Semiconductor Physics and Devices, Second ed., Irwin, Chicago, 1997.
[8] X. Liu, Z. Luo, S. Han, T. Tang, D. Zhang, C. Zhou, Appl. Phys. Lett. 86 (2005) 243501.
[9] C.D. Dimitrakopoulos, A.R. Brown, A. Pomp, J. Appl. Phys. 80 (1996) 2501.
[10] D. Käfer, L. Ruppel, G. Witte, Phys. Rev. B 75 (2007) 085309.
[11] W.S. Hu, Y.T. Tao, Y.J. Hsu, D.H. Wei, Y.S. Wu, Langmuir 21 (2005) 2260.
[12] S.J. Kang, Y. Yi, C.Y. Kim, K.-H. Yoo, A. Moewes, M.H. Cho, J.D. Denlinger, C.N. Whang, G.S. Chang, Phys. Rev. B 72 (2005) 205328.
[13] J.H. Kang, D. da Silva Filho, J.-L. Bredas, X. –Y. Zhu, Appl. Phys. Lett. 86 (2005) 152115.
[14] I. Kymissis, C.D. Dimitrakopoulos, S. Purushothaman, IEEE Trans. Elect. Dev. 48 (2001) 1060.
[15] K. Ihm, B. Kim, T.-H. Kang, K.-J. Kim, M.H. Joo, T.H. Kim, S.S. Yoon, S. Chung, Appl. Phys. Lett. 89 (2006) 033504.
[16] A. Benor, D. Knipp, Org. Electron. 9 (2008) 209.
[17] S.H. Kim, J.H. Lee, S.C. Lim, Y.S. Yang, T. Zyung, Jpn. J. Appl. Phys. 43 (2004) L60.
[18] S. Schiefer, M. Huth, A. Dobrinevski, B. Nickel, J. Am. Chem. Soc. 129 (2007) 10316.
[19] C.-K. Song, B.-W. Koo, S.-B. Lee, D.-H. Kim, Jpn. J. Appl. Phys. 41 (2002) 2730.
[20] J. Zhou, F. Hagelberg, Phys. Rev. Lett. 97 (2006) 045505.
[21] M. Shtein, J. Mapel, J.B. Benziger, S.R. Forrest, Appl. Phys. Lett. 81 (2002) 268.
[22] K.P. Pernstich, S. Haas, D. Oberhoff, C. Goldmann, D.J. Gundlach, B. Batlogg, J. Appl. Phys. 96 (2004) 6431.
[23] B.S. Kim, J.M. Beebe, Y. Jun, X.–Y. Zhu, C.D. Frisbie, J. Am. Chem. Soc. 128 (2006) 4970.
[24] N.J. Watkins, Y. Gao, J. Appl. Phys. 94 (2003) 1289.